Undesirable Oscillations of Phase Locked Loop-Based Position and Speed Estimator for Sensorless Control

Guangqi Li, Yongheng Yang, *Senior Member, IEEE*, Zhiyong Dai, *Senior Member, IEEE*, Yiyun Zhao, Bingqiang Li, and Jin Huang

***Abstract*—Phase-locked loops (PLL) are increasingly used for position and speed estimation in speed sensorless control of permanent-magnet synchronous motors. In this article, the saddle point characteristic phase-portrait is developed to explore the undesirable oscillation phenomena of PLL-based position and speed estimators for speed sensorless control. First, the large-signal model of the PLL-based position and speed estimator is established. Then, the saddle point phase-portrait method and Lyapunov-based argument are adopted to characterize its performance. It is revealed that the PLL-based position and speed estimator has infinite convergence regions. When the system state jumps from one convergence region to another, it will induce undesirable oscillations. Experimental tests are provided to verify the effectiveness of the proposed saddle point characteristic phase-portrait-based analysis.**

***Index Terms*—Permanent-magnet synchronous motor (PMSM), position and speed estimator, saddle point characteristic phase-portrait, speed sensorless control.**

I. Introduction

PERMANENT magnet synchronous machines (PMSMs) have been broadly employed in industrial applications due to the merits like high power density, high efficiency, and low maintenance cost [1], [2], [3], [4]. In high-performance PMSM drives, it is necessary to obtain high precision information of the rotor speed and position. And, the position and speed information is generally achieved by the mechanical position sensors installed on the rotor shaft. However, the use of mechanical position sensor brings several issues in PMSMs, such as increasing system costs, reducing system reliability, and limiting application fields. Thus, sensorless control has been widely discussed in past decades [5], [6], [7], [8].

Recently, many sensorless control methods have been developed for the PMSMs, such as the high frequency signal injection, the electromotive force (EMF) and flux excitation [9], [10], [11], [12], [13], [14]. In these methods, position and speed estimators are of importance, and the essential position and speed information is obtained through the estimator.

To achieve position and speed information, a number of effective methods are developed, e.g., the arctan calculation function, the phase-locked loop (PLL), and the Luenberger observer [15], [16], [17], [18]. Among them, the PLL-based estimator is one of the most classical position and speed estimators. Due to its simple structure and good steady-state accuracy, the PLL-based estimator is increasingly used in the speed sensorless control of PMSM systems. The PLL-based estimator is nonlinear, and it is difficult to analyze the performance in the nonlinear framework. To this end, many small-signal analysis methods are provided to discuss its stability and steady-state accuracy by linearizing the PLL estimator [19], [20], [21], [22]. However, the small-signal analysis methods are only available for the case that speed jumps are small. In many industrial applications, such as compressors, electromechanical brake systems, flywheels, and urban subway traction systems, the motor speed changes largely [23], [24], [25]. In this case, the small-signal analysis methods are inaccurate.

In this article, the large-signal analysis is proposed for the PLL-based speed and position estimator, and accordingly, the conditions of the undesirable oscillations are explored. First, the large-signal model of the PLL-based estimator is established in this article. Then, the saddle point characteristic phase-portrait and Lyapunov-based argument are adopted to explore the undesirable oscillation phenomena of the PLL-based position and speed estimator for speed sensorless control. It is revealed from the exploration that the PLL-based position and speed estimator has infinite stable points and for each stable point, the PLL-based estimator has a convergence region. However, when

Manuscript received 13 October 2022; revised 5 February 2023; accepted 2 April 2023. Date of publication 7 April 2023; date of current version 19 May 2023. This work was supported in part by the NSF of China under Grants 52177192, 52035010 and 52107212; in part by Shaanxi Innovation Team Project 2018TD-012, in part by the Shaanxi international science and technology cooperation project under Grant 2021KWZ-21; in part by the Shaanxi science fund for Distinguished Young Scholars under Grant 2022JC-32; in part by the Shaanxi key laboratory for safety monitoring of food and drug SXKLFDM202203; in part by the fundamental research funds for the central universities under Grant ZYTS23015; in part by the Zhejiang Kunpeng Investigator Program, in part by the Natural Science Basic Research Program of Shaanxi under Grant 2021JQ-703; in part by Xi'an Science and Technology Plan under Grant 21XJZZ0073, and in part by the key laboratory of industrial internet of things & networked control, Ministry of Education 2022FF10. Recommended for publication by Associate Editor H. Hofmann. *(Corresponding author: Zhiyong Dai.)*

Guangqi Li, Zhiyong Dai, and Jin Huang are with the School of Mechanical and Electrical Engineering, Xidian University, Xi'an 710071, China. (e-mail: gqli@xidian.edu.cn; zydai@xidian.edu.cn; jhuang@mail.xidian.edu.cn).

Yongheng Yang is with the College of Electrical Engineering, Zhejiang University, Hangzhou 310027, China. (e-mail: yoy@zju.edu.cn).

Yiyun Zhao and Bingqiang Li are with the School of Automation, Northwestern Polytechnical University, Xi'an 710129, China. (e-mail: zhaoyiyun@mail.nwpu.edu.cn; libingqiang@nwpu.edu.cn).

Color versions of one or more figures in this article are available at https://doi.org/10.1109/TPEL.2023.3265390.

Digital Object Identifier 10.1109/TPEL.2023.3265390

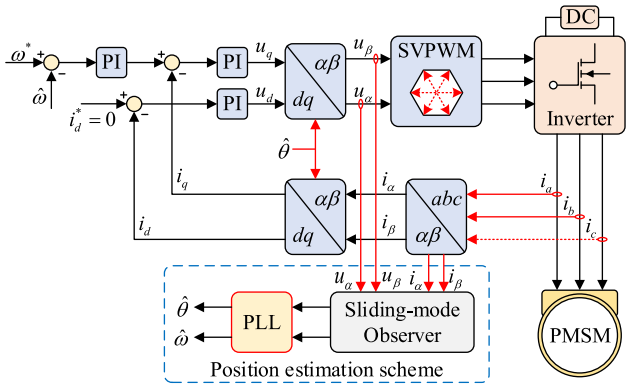

Fig. 1. PMSM sensorless control based on PLLs for position and speed estimation (PI – Proportional-integral; SVPWM – Space vector pulse width modulation).

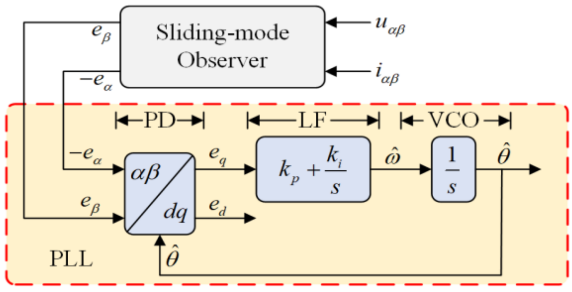

Fig. 2. Structure of the PLL-based position and speed estimator for the PMSM combining with a sliding-mode observer (PD – Phase detector: LF – Loop filter; and VCO – Voltage controlled oscillator).

the system state jumps from one convergence region to another, it will converge to another stable point that is far away from original stable point. This inevitably will introduce undesirable oscillations to the PLL-based position and speed estimator, and eventually deteriorate the performance of the entire PMSM system using the estimator.

The rest of this article is organized as follows. Section II reviews the PLL-based speed and position estimator for the speed sensorless control applications. In Section III, the large-signal analysis for the PLL-based position and speed estimator is proposed, and then, its global performance analysis is given in detail. The analysis can be of usefulness to the design of practical robust PLL-based estimator for speed sensorless control applications. Experimental results are presented in Section IV to verify the theoretical analysis. Finally, Section V concludes the article.

II. PLL-Based Speed and Position Estimation for Speed Sensorless Control

This section provides a review of the PMSM sensorless control with the PLL-based position and speed estimator. The overall control scheme is shown in Fig. 1. Consider the PMSM model in the $\alpha-\beta$ reference frame

$$\begin{bmatrix}\dot{i}_\alpha\\ \dot{i}_\beta\end{bmatrix} = \frac{1}{L_s}\begin{bmatrix}u_\alpha\\ u_\beta\end{bmatrix} - \frac{1}{L_s}\begin{bmatrix}R_s & 0\\ 0 & R_s\end{bmatrix}\begin{bmatrix}i_\alpha\\ i_\beta\end{bmatrix} - \frac{1}{L_s}\begin{bmatrix}e_\alpha\\ e_\beta\end{bmatrix} \tag{1}$$

with

$$\begin{aligned} e_\alpha &= -\lambda_f \omega \sin\theta \\ e_\beta &= \lambda_f \omega \cos\theta \end{aligned} \tag{2}$$

where u_α, u_β, i_α, i_β, e_α, and e_β represent the voltages, currents, and the back EMF of the PMSM in the α- and β-axis, respectively; R_s is the stator resistance; L_s is the stator inductance; λ_f is the magnetic flux; θ and ω are the rotor angle and electric angular velocity, respectively.

According to (2), it has been established that the back EMF contains information about the rotor position and speed of PMSMs, which can be utilized to estimate the same. In the conventional solutions, the following sliding-mode observer is designed to obtain the back EMF of the PMSM

$$\begin{aligned} p\begin{bmatrix}\hat{i}_\alpha\\ \hat{i}_\beta\end{bmatrix} &= \frac{1}{L_s}\begin{bmatrix}u_\alpha\\ u_\beta\end{bmatrix} - \frac{1}{L_s}\begin{bmatrix}R_s & 0\\ 0 & R_s\end{bmatrix}\begin{bmatrix}\hat{i}_\alpha\\ \hat{i}_\beta\end{bmatrix} \\ &\quad - \frac{1}{L_s}\begin{bmatrix}k\,\mathrm{sgn}(\hat{i}_\alpha - i_\alpha)\\ k\,\mathrm{sgn}(\hat{i}_\beta - i_\beta)\end{bmatrix} \end{aligned} \tag{3}$$

$$\hat{e}_\alpha = \frac{\omega_f}{s+\omega_f} k\,\mathrm{sgn}(\hat{i}_\alpha - i_\alpha)$$

$$\hat{e}_\beta = \frac{\omega_f}{s+\omega_f} k\,\mathrm{sgn}(\hat{i}_\beta - i_\beta) \tag{4}$$

in which $\hat{i}_\alpha$ and $\hat{i}_\beta$, $\hat{e}_\alpha$ and $\hat{e}_\beta$ are the estimated stator currents and the back-EMF, respectively; sgn$(\cdot)$ is the sign function. According to the analysis and discussions in [26], the sliding-mode observer given in (3) and (4) can effectively estimate the back-EMF.

When the back-EMF is obtained, the PLL is the conventional method to estimate the position and speed of the PMSMs. Fig. 2 shows the general structure of the PLL, including a phase detector (PD), a loop filter (LF), and a voltage-controlled oscillator (VCO). With a small-signal analysis, the stability and steady-state accuracy of the PLL-based estimator are well discussed in [22]. However, the small-signal analysis for the PLL-based estimator is accurate only under the condition that the difference between the speed and its estimation is sufficiently small, i.e., $\omega \approx \hat{\omega}$. In certain applications, where the motor speed always changes widely, this condition is then not satisfied. In this case, the small-signal analysis for the PLL-based estimator is inaccurate. To deal with this issue, the saddle point characteristic phase-portrait is proposed in the next section. The characterization has revealed that undesirable oscillations of the PLL-based position and speed estimator will occur in certain cases of large speed changes.

III. Saddle Point Characteristic Phase-Portrait Analysis

In this section, a global performance analysis for the PLL-based position and speed estimator of the PMSM is proposed.

First, the large-signal model of the PLL-based position and speed estimator is established. Then, the saddle point characteristic phase-portrait methods and Lyapunov-based argument are adopted to show the global performance of the PLL-based position and speed estimator.

A. Large-Signal Model

Fig. 2 shows the structure of the PLL-based position and speed estimator of the PMSM. The inputs of the PD are the EMFs e_α and e_β of the PMSM, which are obtained from the sliding-mode observer, and the EMFs can be expressed as

$$\begin{aligned} e_\alpha &= -\lambda_f \omega \sin\theta \\ e_\beta &= \lambda_f \omega \cos\theta. \end{aligned} \tag{5}$$

Then, from the PD part in the PLL, it is clear that

$$\begin{aligned} e_q &= -e_\alpha \cos\hat{\theta} - e_\beta \sin\hat{\theta} \\ &= \lambda_f \omega \sin\left(\theta - \hat{\theta}\right) \end{aligned} \tag{6}$$

where $\hat{\theta}$ is the estimation of the position θ. According to the LF and the VCO in the PLL shown in Fig. 2, it is deduced that

$$\begin{aligned} \hat{\theta} &= \int \hat{\omega} ds \\ \hat{\omega} &= k_p e_q + k_i \int e_q ds \end{aligned} \tag{7}$$

in which $\hat{\omega}$ is the estimation of the speed ω. It means that

$$\begin{aligned} \dot{\hat{\theta}} &= \hat{\omega} \\ \dot{\hat{\omega}} &= k_p \dot{e}_q + k_i e_q. \end{aligned} \tag{8}$$

Define $\tilde{\theta} = \hat{\theta} - \theta$ and $\tilde{\omega} = \hat{\omega} - \omega$. Then, by using (6) and (8), it has

$$\begin{aligned} \dot{\tilde{\theta}} &= \tilde{\omega} \\ \dot{\tilde{\omega}} &= -k_p \lambda_f \omega \cos\tilde{\theta}\tilde{\omega} - k_i \lambda_f \omega \sin\tilde{\theta} \end{aligned} \tag{9}$$

which is the large-signal model of the PLL-based position and speed estimator of PMSMs. This model can accurately describe the global performance of the PLL. Note that the large-signal model (9) is nonlinear. Hence, the linear analysis methods fail to obtain its global performance. In the following discussions, the nonlinear analysis approaches are adopted to explore its global performance.

B. Global Performance and Undesirable Oscillations

Based on the large-signal model in (9), the saddle point characteristic phase-portrait of the PLL-based position and speed estimator can be obtained, as it is shown in Fig. 3. The way to draw the boundary of the convergence region is provided in the Appendix. According to Fig. 3, it is known that the following.

1) The PLL-based estimator has infinite stable points $(2k\pi, 0)$, $k = 0, \pm1, \pm2, \ldots$. For each stable point, there is a convergence region. For any initial states in a convergence region, the PLL-based position and speed estimator will converge to the unique stable point of that convergence region.
2) When the system states of the PLL-based estimator jump from one convergence region to another, the PLL-based estimator converges to another stable point. This will inevitably induce oscillations that are undesirable.

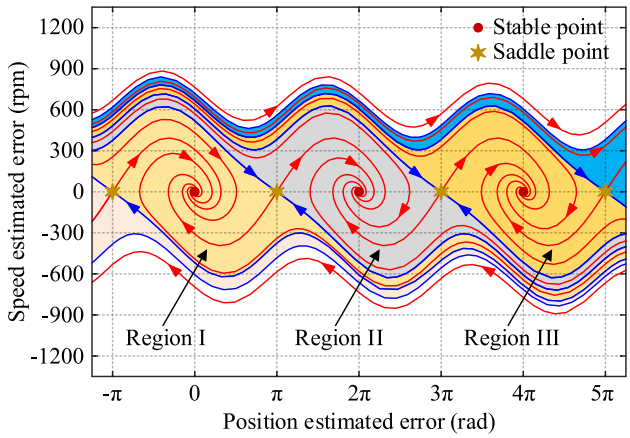

Fig. 3. Phase-portrait of the PLL-based position and speed estimators.

TABLE I
PARAMETERS OF THE SPMSM

Parameter	Value	Parameter	Value
Rated Power (kW)	0.2	Rated Speed (r/min)	3000
Rated Voltage (V)	24	Stator Resistance (Ω)	0.11
Rated Current (A)	12.5	Stator Inductance (mH)	0.19
Rated Torque (N·m)	0.64	Number of Poles	10

A strict theoretical analysis is provided to discuss the above global performance of the PLL-based estimator in the following. According to the definition of the equilibrium point in nonlinear systems, the equilibrium points $(\tilde{\theta}^*, \tilde{\omega}^*)$ of the nonlinear system (9) satisfy

$$\begin{aligned} 0 &= \tilde{\omega}^* \\ 0 &= -k_p \lambda_f \omega \cos\tilde{\theta}^* \tilde{\omega}^* - k_i \lambda_f \omega \sin\tilde{\theta}^*. \end{aligned} \tag{10}$$

A simple calculation implies that the system has infinite equilibrium points, and they are *(nπ,0), n = 0, ±1, ±2* …. The qualitative behavior near these equilibrium points can be derived through linear approximation of the nonlinear system at the equilibrium points. To this end, we define $\tilde{\theta}_n = \tilde{\theta} - n\pi$, $\tilde{\omega}_n = \tilde{\omega} - 0$. From (9), the following linear approximation of the nonlinear system can be obtained:

$$\begin{pmatrix} \dot{\tilde{\theta}}_n \\ \dot{\tilde{\omega}}_n \end{pmatrix} = A_n \begin{pmatrix} \tilde{\theta}_n \\ \tilde{\omega}_n \end{pmatrix} \tag{11}$$

where

$$A_n := \begin{bmatrix} 0 & 1 \\ -k_i \lambda_f \omega \cos(n\pi) & -k_p \lambda_f \omega \cos(n\pi) \end{bmatrix}.$$

When $n = 2k$, $k = 0, \pm1, \pm2$ …, the matrix A_n is

$$A_n := \begin{bmatrix} 0 & 1 \\ -k_i \lambda_f \omega & -k_p \lambda_f \omega \end{bmatrix}$$

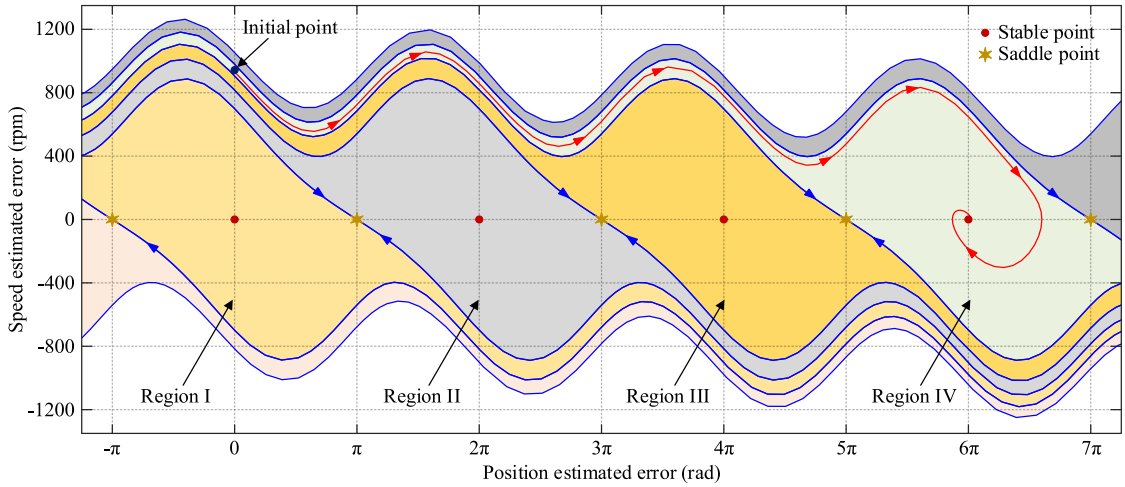

Fig. 4. Undesirable oscillations of the PLL-based position and speed estimators.

which means that A_n has two eigenvalues with negative real part, and the equilibrium points $(2k\pi,\ 0),\ k\ =\ 0,\ \pm1,\ \pm2,\ldots$, are stable points.

When $n = 2k+1,\ k = 0,\ \pm1,\ \pm2,\ \ldots$, the matrix A_n can be expressed as

$$A_n := \begin{bmatrix} 0 & 1 \\ k_i\lambda_f\omega & k_p\lambda_f\omega \end{bmatrix}.$$

A direct calculation implies that A_n has an eigenvalue with positive real part, and the other with negative real part. Hence, the equilibrium points $((2k+1)\pi,\ 0),\ k = 0,\ \pm1,\ \pm2\ldots$, are unstable, and they are called saddle points.

In the following, it is proven that the PLL-based estimator is input-state stability (ISS). In practice, the input of the PLL-based estimator contains disturbances. Without loss of generality, it is assumed that the PLL-based estimator has the disturbance $d(t)$, and the large-signal model of the PLL-based estimator with disturbances is

$$\begin{aligned} \dot{\tilde{\theta}} &= \tilde{\omega} \\ \dot{\tilde{\omega}} &= -k_p\lambda_f\omega\cos\tilde{\theta}\tilde{\omega} - k_i\lambda_f\omega\sin\tilde{\theta} + d(t) \end{aligned} \tag{12}$$

which is nonlinear, and it is difficult to directly construct the Lyapunov function and analyze its stability. Hence, the variable gradient method is introduced to (12) to establish the Lyapunov function. More specifically, let $V(\tilde{\theta},\tilde{\omega})$ be a scalar function, and

$$g(\tilde{\theta},\tilde{\omega}) = \nabla U = \begin{pmatrix} \partial V/\partial\tilde{\theta} \\ \partial V/\partial\tilde{\omega} \end{pmatrix} = \begin{pmatrix} g_1(\tilde{\theta},\tilde{\omega}) \\ g_2(\tilde{\theta},\tilde{\omega}) \end{pmatrix}. \tag{13}$$

The derivative $\dot{V}(t)$ along the trajectories of (12) is

$$\begin{aligned} \dot{V} = {} & g_1(\tilde{\theta},\tilde{\omega})\tilde{\omega} + g_2(\tilde{\theta},\tilde{\omega}) \times (-k_p\lambda_f\omega\cos\tilde{\theta}\tilde{\omega} \\ & - k_i\lambda_f\omega\sin\tilde{\theta}) + g_2(\tilde{\theta},\tilde{\omega})d(t). \end{aligned} \tag{14}$$

The idea of the variable gradient method is to select $g_1(\cdot)$ and $g_2(\cdot)$ such that $g_1(\cdot)$ and $g_2(\cdot)$ are the gradient of a positive definite function $V(\cdot)$, and at the same time, the function $g_1(\cdot)\tilde{\omega} + g_2(\cdot) \times (-k_p\lambda_f\omega\cos\tilde{\theta}\tilde{\omega} - k_i\lambda_f\omega\sin\tilde{\theta})$is negative definite.

Let

$$\begin{aligned} g_1(\cdot) &= \alpha(\tilde{\theta})\tilde{\theta} + \beta\tilde{\omega} \\ g_2(\cdot) &= \beta\tilde{\theta} + \delta\tilde{\omega} \end{aligned} \tag{15}$$

where the scalar function $\alpha(\cdot)$ and constants β, δ are to be determined. Then, it has

$$\begin{aligned} & g_1(\cdot)\tilde{\omega} + g_2(\cdot) \times (-k_p\lambda_f\omega\cos\tilde{\theta}\tilde{\omega} - k_i\lambda_f\omega\sin\tilde{\theta}) \\ & = \alpha(\tilde{\theta})\tilde{\theta}\tilde{\omega} + \beta\tilde{\omega}^2 - \beta k_p\lambda_f\omega\cos\tilde{\theta}\tilde{\omega}\tilde{\theta} - \beta k_i\lambda_f\omega\sin\tilde{\theta}\tilde{\theta} \\ & \quad - \delta k_p\lambda_f\omega\cos\tilde{\theta}\tilde{\omega}^2 - \delta\beta k_i\lambda_f\omega\sin\tilde{\theta}\tilde{\omega} \\ & = -\beta k_i\lambda_f\omega\sin\tilde{\theta}\tilde{\theta} - (\delta k_p\lambda_f\omega\cos\tilde{\theta} - \beta)\tilde{\omega}^2 \\ & \quad + \tilde{\omega}\left[\alpha(\tilde{\theta})\tilde{\theta} - \beta k_p\lambda_f\omega\cos\tilde{\theta}\tilde{\theta} - \delta\beta k_i\lambda_f\omega\sin\tilde{\theta}\right]. \end{aligned} \tag{16}$$

Choosing $\alpha(\tilde{\theta})\tilde{\theta}$ such that

$$\alpha(\tilde{\theta})\tilde{\theta} = \beta k_p\lambda_f\omega\cos\tilde{\theta}\tilde{\theta} + \delta\beta k_i\lambda_f\omega\sin\tilde{\theta} \tag{17}$$

results in

$$\begin{aligned} & g_1(\cdot)\tilde{\omega} + g_2(\cdot) \times \left(-k_p\lambda_f\omega\cos\tilde{\theta}\tilde{\omega} - k_i\lambda_f\omega\sin\tilde{\theta}\right) \\ & = -\beta k_i\lambda_f\omega\sin\tilde{\theta}\tilde{\theta} - \left(\delta k_p\lambda_f\omega\cos\tilde{\theta} - \beta\right)\tilde{\omega}^2. \end{aligned} \tag{18}$$

According to (15) and (17), the function $V(\cdot)$ is obtained as

$$\begin{aligned} V(\cdot) &= \int_0^{\tilde{\theta}} g_1(y_1, 0)\, dy_1 + \int_0^{\tilde{\omega}} g_2\left(\tilde{\theta}, y_2\right) dy_2 \\ &= \beta k_p\lambda_f\omega\int_0^{\tilde{\theta}} y_1\cos y_1 dy_1 + \beta\tilde{\theta}\tilde{\omega} \\ &\quad + \delta\beta k_i\lambda_f\omega\int_0^{\tilde{\theta}}\sin y_1 dy_1 + \frac{1}{2}\delta\tilde{\omega}^2. \end{aligned} \tag{19}$$

It is easy to check that

$$\begin{aligned} \frac{\partial V}{\partial\tilde{\theta}} &= \beta k_p\lambda_f\omega\cos\tilde{\theta}\tilde{\theta} + \delta\beta k_i\lambda_f\omega\sin\tilde{\theta} + \beta\tilde{\omega} \\ \frac{\partial V}{\partial\tilde{\omega}} &= \beta\tilde{\theta} + \delta\tilde{\omega} \end{aligned} \tag{20}$$

TABLE II
EXPERIMENTAL CONDITIONS

Case	Conditions	Convergence region	With/without oscillations
Case A	speed jump from 2500 to 2000 r/min	Region I	Without oscillations
Case B	speed jump from 2500 to 1200 r/min	Region V	With oscillations

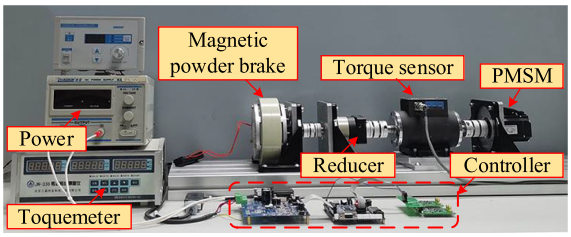

Fig. 5. Photo of the experimental platform.

which means that $g_1(\cdot)$ and $g_2(\cdot)$ are the gradient functions of the scale function $V(\cdot)$.

Next, it is shown that there are positive constants β and δ such that the function $V(\cdot)$ is positive definite, and $g_1(\cdot)\tilde{\omega} + g_2(\cdot) \times (-k_p\lambda_f\omega\cos\tilde{\theta}\tilde{\omega} - k_i\lambda_f\omega\sin\tilde{\theta})$ is negative definite. A simple calculation implies that

$$V(\cdot) \geq \frac{1}{2}\beta k_p\lambda_f\omega\tilde{\theta}^2 + \beta\tilde{\theta}\tilde{\omega} + \frac{1}{2}\delta\tilde{\omega}^2$$

$$\dot{V}(\cdot) \leq -\frac{1}{4}\beta k_i\lambda_f\omega\tilde{\theta}^2 - \frac{1}{4}\left(\delta k_p\lambda_f\omega - 4\beta\right)\tilde{\omega}^2 + cd(t)^2$$

where c is a positive constant. Hence, choosing

$$\beta > 0, \text{and}\delta > \frac{4\beta}{k_p\lambda_f\omega} \tag{21}$$

results in that the function $V(\cdot)$ is positive definite, and $g_1(\cdot)\tilde{\omega} + g_2(\cdot) \times (-k_p\lambda_f\omega\cos\tilde{\theta}\tilde{\omega} - k_i\lambda_f\omega\sin\tilde{\theta})$ is negative definite. It means that the PLL-based estimator is ISS in the stable point $(0,\ 0)$. For other stable points, the same Lyapunov-based argument can be provided to show its stability.

The above stability analysis shows that for each stable point, there is a convergence region, and for any initial states that belong to this convergence region, the PLL-based estimator is ISS. In addition, when $d(t) = 0$, it is easy to prove $\lim_{t\to\infty}\tilde{\theta}\,(t) = 0$ and $\lim_{t\to\infty}\tilde{\omega}\,(t) = 0$. Hence, for any initial states belonging to this convergence region, the PLL-based estimator will converge to the unique stable point of this convergence region. However, when the system state of the PLL-based estimator jumps from one convergence region to another, it will converge to the stable point that is far away from its original stable point. This will cause undesirable oscillations. For instance, as shown in Fig. 4, a rotor speed jumps from 1750 to 800 r/min, the states of the PLL-based estimator go from the convergence region I to the convergence region IV. Then, the PLL-based estimator converges to the stable point in the convergence region IV, and it endures several undesirable oscillations and presents rather slow dynamics.

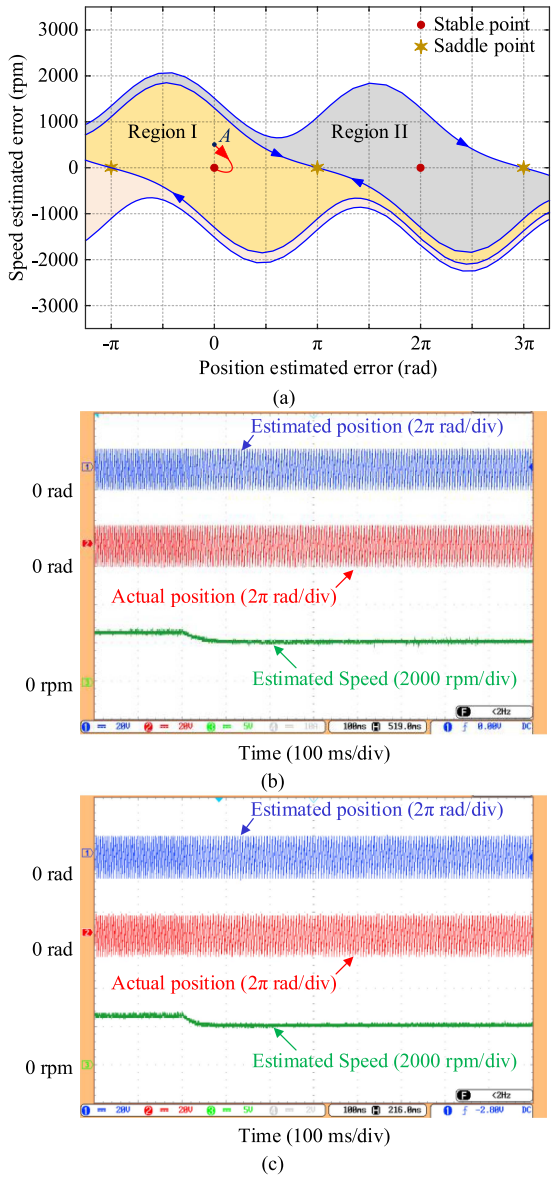

Fig. 6. Experimental results of the system under case A. (a) Saddle point characteristic phase-portrait, when measured position and speed are used in closed-loop control. (b) When the measured position and speed are used in the closed-loop control. (c) When the estimated position and speed are used in the closed-loop control.

IV. EXPERIMENTAL RESULTS

In this section, the experiments are performed to verify the above discussion. Fig. 5 is the experimental platform. The 0.2-kW PMSM is selected as the target machine and its parameters are listed in Table I. The magnetic powder brake (SKISIA PB-1.2) provides the load torque, which is mechanically connected to the target machine. The digital signal

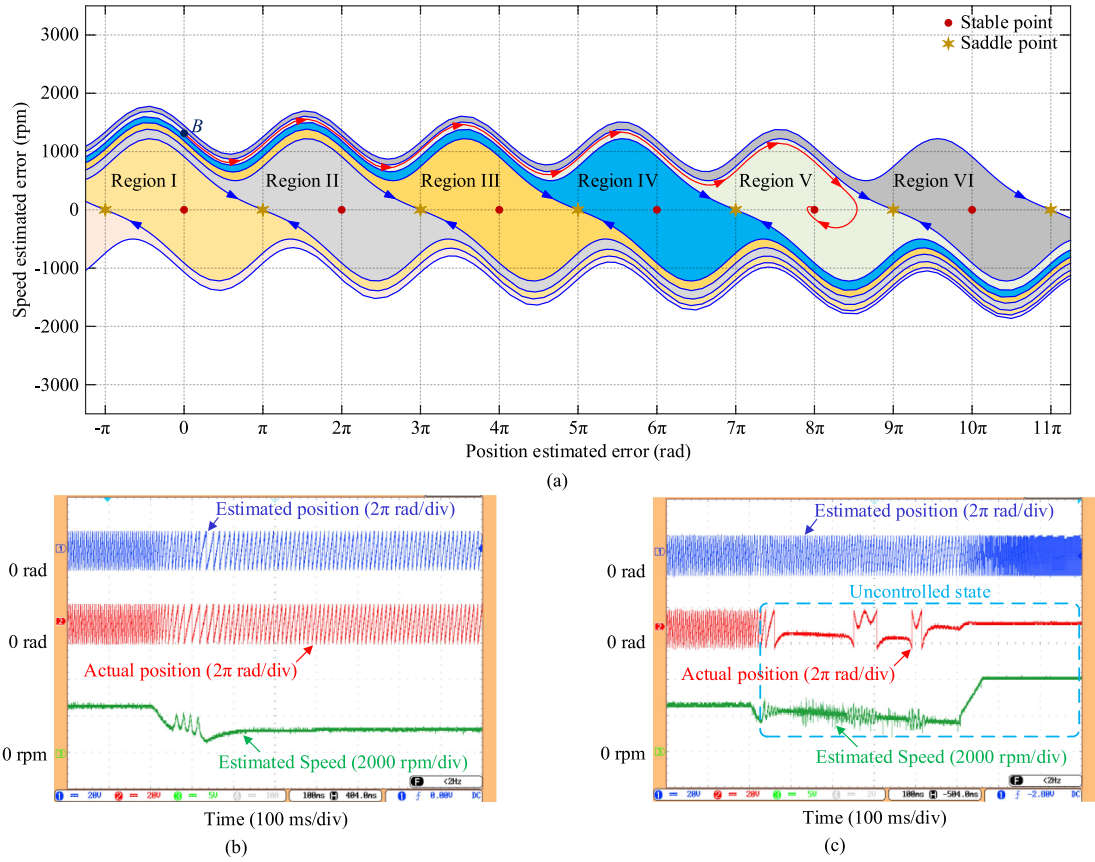

Fig. 7. Experimental results of the system under case B. (a) Saddle point characteristic phase-portrait, when the measured position and speed are used in closed-loop control. (b) When the measured position and speed are used in the closed-loop control. (c) When the estimated position and speed are used in the closed-loop control.

processor TMS320F28335 has been implemented to execute the control algorithms. N-Channel Power MOSFET, IPD200N15N3 G, constitutes the voltage inverter, and the PWM switching frequency of the inverter is 10 kHz. The dc-link voltage is set as 24 V. An incremental encoder with 2500 PPR is utilized to acquire the actual rotor position and motor speed for comparison. The data storage oscilloscope, GDS-2104A, is used to record the experimental results. The current and speed loop operation frequencies are 10 and 5 kHz, respectively. The parameters of the speed PI regulator are $k_{sp} = 1.5$ and $k_{si} = 0.02$, respectively. The parameters of the current PI regulator are $k_{cp} = 1$ and $k_{ci} = 0.025$, respectively. The parameters of the PLL-based estimator are $k_p = 92$ and $k_i = 0.4232$. The PLL-based senorless control scheme is tested under the two cases given in Table II.

Fig. 6 shows the experimental results under case A. In this case, the speed reference jumps from 2500 to 2000 r/min. Fig. 6(a) is the saddle point characteristic phase-portrait of the PLL-based estimator, when the measured position and speed are used in the speed and current controllers. It is observed that, even when the system states change, the state $(\tilde{\theta}(\mathrm{t}), \tilde{\omega}(\mathrm{t}))$ still belongs to region I and hence no oscillations emerge. Fig. 6(b) shows the estimated speed and the back EMF by the PLL-based estimator when the measured position and speed are used in the closed-loop control. From Fig. 6(b), there are no oscillations of the position and speed estimator, and it confirms the analysis in Fig. 6(a). Fig. 6(c) presents the sensorless control experimental results when the estimated position and speed are used in the closed-loop control. Since no oscillations occur in the PLL-based estimator, the sensorless control of the PMSM achieves a good performance.

In case B, the speed reference jumps from 2500 to 1200 r/min. The experimental results under case B are provided in Fig. 7. Fig. 7(a) is the saddle point characteristic phase-portrait of the PLL-based estimator in this case, when the measured position and speed are used in the closed-loop control. Observations in Fig. 7(a) indicate that the states $(\tilde{\theta}(\mathrm{t}), \tilde{\omega}(\mathrm{t}))$ jump from region I to region V, and the PLL-based estimator converges to the stable point of region V. Although the actual position and speed can be estimated through the PLL-based position and speed estimator, the estimator has several undesirable oscillations in the estimation process. In addition, Fig. 7(b) shows the actual position, and the estimated position and speed by the PLL-based estimator when the measured position and speed are used in the closed-loop control. According to Fig. 7(b), it is known that the actual position and speed can be estimated through the PLL-based position and speed estimator. However, in the estimation process, certain undesirable oscillations occur when the system state jumps from one convergence region to another.

To further demonstrate the impact of the oscillations, the measured position and speed are replaced by the estimated

position and speed in the closed-loop control, and the experimental results are shown in Fig. 7(c). From Fig. 7(c), it is known that the undesirable oscillations seriously deteriorate the performance of the sensorless control, and the PMSM goes to uncontrollable state, and eventually, stops.

In summary, when the states do not jump out the convergence region, the PLL-based estimator can obtain the information of the position and speed of the PMSMs with fast dynamics, and the PLL-based estimator realizes the sensorless control well. Unfortunately, when the states jump out of the convergence region, the PLL-based estimator presents many oscillations that are undesirable, and it will significantly deteriorate the performance of the sensorless control. In these cases, the PMSM may be uncontrollable and even stop in operation.

V. Conclusion

The large-signal analysis for the PLL-based position and speed estimator has been provided in this article. The saddle point characteristic phase-portrait method and Lyapunov-based argument have been adopted to analyze its global performance under large speed variations/changes. This can be the guidelines for designing robust PLLs for the speed sensorless control. The main contributions of this article are concluded as follows.

1) The PLL-based speed estimation in sensorless control has infinite stable points and saddle points. For each stable point, the PLL-based speed estimator has a convergence region. When the initial state belongs to this convergence region, the PLL-based estimator will converge to the unique stable point of this convergence region.
2) When the system states of the PLL-based estimator jump from one convergence region to another, it causes undesirable oscillations. These undesirable oscillations will deteriorate the performance of the sensorless control significantly, and the entire machine may go to an uncontrollable state or stop.

Appendix

The way to draw the boundary of the convergence region for the PLL-based position and speed estimator is provided in this section. In details the boundary can be drawn as follows.

Step 1: For the large-signal model of the PLL-based estimator, $\begin{matrix}\dot{\tilde{\theta}} = \tilde{\omega} \\ \dot{\tilde{\omega}} = -k_p\lambda_f\omega\cos\tilde{\theta}\tilde{\omega} - k_i\lambda_f\omega\sin\tilde{\theta}\end{matrix}$, find all equilibrium points.

Step 2: For saddle points, use linearization to obtain the saddle point characteristics. Specifically, let the eigenvalues of the matrix $A_n = \begin{bmatrix} 0 & 1 \\ k_i\lambda_f\omega & k_p\lambda_f\omega \end{bmatrix}$ be $\lambda_1 > 0 > \lambda_2$ and the corresponding eigenvectors be v_1 and v_2.

Step 3: The boundary of the convergence region is drawn by solving the equation in a backward way

$$\begin{matrix} \dot{\tilde{\theta}} & = & \tilde{\omega} \\ \dot{\tilde{\omega}} & = & -k_iV\sin\tilde{\theta} - k_pV\tilde{\omega}\cos\tilde{\theta} \\ (\tilde{\theta}(0),\tilde{\omega}(0))^T & = & = ((2k+1)\pi,0)^T \pm \alpha v_2 \end{matrix}.$$

That is, solving the equation in the forward way

$$\begin{matrix} \dot{\tilde{\theta}} & = & -\tilde{\omega} \\ \dot{\tilde{\omega}} & = & k_iV\sin\tilde{\theta} + k_pV\tilde{\omega}\cos\tilde{\theta} \\ (\tilde{\theta}(0),\tilde{\omega}(0))^T & = & = ((2k+1)\pi,0)^T \pm \alpha v_2 \end{matrix}.$$

References

[1] C. Gong, Y. Hu, J. Gao, Y. Wang, and L. Yan, "An improved delay-suppressed sliding-mode observer for sensorless vector-controlled PMSM," *IEEE Trans. Ind. Electron.*, vol. 67, no. 7, pp. 5913–5923, Jul. 2020.

[2] K. Zhang, M. Fan, Y. Yang, Z. Zhu, C. Garcia, and J. Rodriguez, "An improved adaptive selected harmonic elimination algorithm for current measurement error correction of PMSMs," *IEEE Trans. Power Electron.*, vol. 36, no. 11, pp. 13128–13138, Nov. 2021.

[3] F. Wang, L. He, and J. Rodriguez, "FPGA-based continuous control set model predictive current control for PMSM system using multistep error tracking technique," *IEEE Trans. Power Electron.*, vol. 35, no. 12, pp. 13455–13464, Dec. 2020.

[4] C. Wu, Z. Chen, and Q. Chen, "Hybrid-modulation-based full-speed sensorless control for permanent magnet synchronous motors," *IEEE Trans. Power Electron.*, vol. 37, no. 5, pp. 5908–5917, May 2022.

[5] S.-K. Sul, Y.-C. Kwon, and Y. Lee, "Sensorless control of IPMSM for last 10 years and next 5 years," *CES Trans. Elect. Mach. Syst.*, vol. 1, no. 2, pp. 91–99, Jun. 2017.

[6] J. Yoo, J. Lee, and S.-K. Sul, "Analysis of instability in torque control of sensorless PMSM drives in flux weakening region," *IEEE Trans. Power Electron.*, vol. 36, no. 9, pp. 10815–10826, Sep. 2021.

[7] D. Xu, B. Wang, G. Zhang, G. Wang, and Y. Yu, "A review of sensorless control methods for AC motor drives," *CES Trans. Elect. Mach. Syst.*, vol. 2, no. 1, pp. 104–115, Mar. 2018.

[8] A. Apte, V. A. Joshi, H. Mehta, and R. Walambe, "Disturbance-observer-based sensorless control of PMSM using integral state feedback controller," *IEEE Trans. Power Electron.*, vol. 35, no. 6, pp. 6082–6090, Jun. 2020.

[9] G. Wang, M. Valla, and J. Solsona, "Position sensorless permanent magnet synchronous machine drives—A review," *IEEE Trans. Ind. Electron.*, vol. 67, no. 7, pp. 5830–5842, Jul. 2020.

[10] G. Zhang, G. Wang, H. Wang, D. Xiao, L. Li, and D. G. Xu, "Pseudo-random-frequency sinusoidal injection-based sensorless IPMSM drives with tolerance for system delays," *IEEE Trans. Power Electron.*, vol. 34, no. 4, pp. 3623–3632, Apr. 2019.

[11] X. Jin, R. Ni, W. Chen, F. Blaabjerg, and D. Xu, "High-frequency voltage-injection methods and observer design for initial position detection of permanent magnet synchronous machines," *IEEE Trans. Power Electron.*, vol. 33, no. 9, pp. 7971–7979, Sep. 2018.

[12] Z. Chen, A. A. Dawara, X. Zhang, H. Zhang, C. Liu, and G. Luo, "Adaptive sliding mode observer-based sensorless control for SPMSM employing a dual-PLL," *IEEE Trans. Transp. Electrific.*, vol. 8, no. 1, pp. 1267–1277, Mar. 2022.

[13] L. Qu, W. Qiao, and L. Qu, "An enhanced linear active disturbance rejection rotor position sensorless control for permanent magnet synchronous motors," *IEEE Trans. Power Electron.*, vol. 35, no. 6, pp. 6175–6184, Jun. 2020.

[14] W. Xu, Y. Jiang, C. Mu, and F. Blaabjerg, "Improved nonlinear flux observer-based second-order SOIFO for PMSM sensorless control," *IEEE Trans. Power Electron.*, vol. 34, no. 1, pp. 565–579, Jan. 2019.

[15] C. Lascu and G.-D. Andreescu, "PLL position and speed observer with integrated current observer for sensorless PMSM drives," *IEEE Trans. Ind. Electron.*, vol. 67, no. 7, pp. 5990–5999, Jul. 2020.

[16] G. Zhang, G. Wang, D. Xu, and N. Zhao, "ADALINE-network-based PLL for position sensorless interior permanent magnet synchronous motor drives," *IEEE Trans. Power Electron.*, vol. 31, no. 2, pp. 1450–1460, Feb. 2016.

[17] Z. Yin, Y. Zhang, X. Cao, D. Yuan, and J. Liu, "Estimated position error suppression using novel PLL for IPMSM sensorless drives based on full-order SMO," *IEEE Trans. Power Electron.*, vol. 37, no. 4, pp. 4463–4474, Apr. 2022.

[18] A. Andersson and T. Thiringer, "Motion sensorless IPMSM control using linear moving horizon estimation with Luenberger observer state feedback," *IEEE Trans. Transp. Electrific.*, vol. 4, no. 2, pp. 464–473, Jun. 2018.

[19] S. Golestan, M. Monfared, and F. D. Freijedo, "Design-oriented study of advanced synchronous reference frame phase-locked loops," *IEEE Trans. Power Electron.*, vol. 28, no. 2, pp. 765–778, Feb. 2013.
[20] M. H. Bierhoff, "A general PLL-type algorithm for speed sensorless control of electrical drives," *IEEE Trans. Ind. Electron.*, vol. 64, no. 12, pp. 9253–9260, Dec. 2017.
[21] H. Wang, X. Ge, Y. Yue, and Y.-C. Liu, "Dual phase-locked loop-based speed estimation scheme for sensorless vector control of linear induction motor drives," *IEEE Trans. Ind. Electron.*, vol. 67, no. 7, pp. 5900–5912, Jul. 2020.
[22] H. Wang, Y. Yang, X. Ge, Y. Zuo, Y. Yue, and S. Li, "PLL- and FLL-based speed estimation schemes for speed-sensorless control of induction motor drives: Review and new attempts," *IEEE Trans. Power Electron.*, vol. 37, no. 3, pp. 3334–3356, Mar. 2022.
[23] X. Chen, R. Sun, W. Jiang, Q. Jia, and J. Zhang, "A novel two-stage extended Kalman filter algorithm for reaction flywheels fault estimation," *Chin. J. Aeronaut.*, vol. 29, no. 2, pp. 462–469, Apr. 2016.
[24] Z. Xu and C. Gerada, "Enhanced force estimation for electromechanical brake actuators in transportation vehicles," *IEEE Trans. Power Electron.*, vol. 36, no. 12, pp. 14329–14339, Dec. 2021.
[25] F. Zhao, Z. Yu, J. Cao, and L. Li, "Design and optimization of a high-speed permanent magnet synchronous machine for gas compressors," *IEEE Trans. Magn.*, vol. 58, no. 2, Feb. 2022, Art. no. 8100905.
[26] Z. Qiao, T. Shi, Y. Wang, Y. Yan, C. Xia, and X. He, "New sliding-mode observer for position sensorless control of permanent-magnet synchronous motor," *IEEE Trans. Ind. Electron.*, vol. 60, no. 2, pp. 710–719, Feb. 2013.

Guangqi Li received the B.S. degree in applied mathematics from Lanzhou University, Lanzhou, China, in 2009, the M.S. degrees in applied mathematics from Xiangtan University, Xiangtan, China, in 2012, and the Ph.D. degree in control theory and control engineering from Beihang University, Beijing, China, in 2017.

He is currently an Assistant Professor with the School of Mechanical and Electrical Engineering, Xidian University, Xi'an, China. His research interests include nonlinear analysis, nonlinear control, power electronics and motion control.

Yongheng Yang (Senior Member, IEEE) received the B.Eng. degree in electrical engineering and automation from Northwestern Polytechnical University, Xi'an, China, in 2009, and the Ph.D. degree in energy technology from Aalborg University, Denmark, in 2014.

He was a Visiting Scholar at Texas A&M University, USA, during March 2013–May 2013. From 2014 to 2020, he was associated with the Department of Energy Technology, Aalborg University, where he achieved the rank of tenured an Associate Professor in 2018. In January 2021, he was a Professor with Zhejiang University. He was a Zhejiang Kunpeng Investigator in 2023. His research interests include grid-integration of photovoltaic systems and control of power converters, specifically grid-forming control technologies.

Dr. Yang was the Chair of the IEEE Denmark Section in 2019–2020 and an Associate Editor for several IEEE Transactions. He was the recipient of the 2018 IET Renewable Power Generation Premium Award and was recognized as an Outstanding Reviewer for the IEEE Transactions on Power Electronics in 2018. He was the recipient of the 2021 Richard M. Bass Outstanding Young Power Electronics Engineer Award from the IEEE Power Electronics Society and the 2022 IEEJ Isao Takahashi Power Electronics Award. In addition, he has received two IEEE Best Paper Awards. He was included on the list of the Highly Cited Chinese Researchers by Elsevier in 2022–2023. He is currently theVice Chair of the IEEE PELS Technical Committee on Sustainable Energy Systems and a Council Member of the China Power Supply Society.

Zhiyong Dai (Senior Member, IEEE) received the B.S. and M.S. degrees in electrical engineering and the Ph.D. degree in detection technology and automation device from Northwestern Polytechnical University, Xi'an, China, in 2009, 2012, and 2016, respectively.

From 2014 to 2016, he was a Visiting Ph.D. Student with the Department of Electrical Engineering and Computer Science, Case Western Reserve University, Cleveland, OH, USA. He is currently an Associate Professor with the School of Mechanical and Electrical Engineering, Xidian University, Xi'an, China. His research interests include power electronics and motion control.

Yiyun Zhao received the B.E. degree in electrical engineering in 2017 from Northwestern Polytechnical University, Xi'an, China, where he is currently working toward the Ph.D. degree with the School of Automation, Northwestern Polytechnical University.

His research interests include more electric aircraft, nonlinear control, and mechatronic servo control.

Bingqiang Li received the B.E. and M.E. degrees in electrical engineering and the Ph.D. degree in control science and engineering from Northwestern Polytechnical University, Xi'an, China, in 2004, 2007, and 2010, respectively.

He is currently a Professor and the Dean of the Department of Electrical Engineering, Northwestern Polytechnical University. His research interests include more electric aircraft, iterative learning control, servo control, multiagent systems and their applications.

Jin Huang received the Ph.D. degree in mechanical engineering from Xidian University, Xi'an, China, in 1999.

He was with the Department of Mechanical Engineering, University of British Columbia, Vancouver, BC, Canada, as a Visiting Researcher, during 2001–2002. He is currently a Professor and the Dean of the School of ElectroMechanical Engineering, Xidian University, and the Director of the Key Laboratory of Electronic Equipment Design, Minister of Education. He has authored or coauthored more than 100 papers in various peer reviewed journals and conference proceedings, and he holds more than 50 patents. His research interests include flexible electronics, mechatronics, and three-dimensional printing.

Dr. Huang is the Fellow of Chinese Institute of Electronics and the Deputy Secretary General of Electromechanical Engineer Society of China.